© 2020. Published by The Company of Biologists Ltd | Journal of Cell Science (2020) 133, jcs234385. doi:10.1242/jcs.234385

RESEARCH ARTICLE

Abl-mediated PI3K activation regulates macrophage podosome formation

Yuhuan Zhou, Zhen Feng, Fakun Cao, Xiaoting Liu, Xiaojie Xia and Cheng-han Yu*

ABSTRACT

Podosomes play crucial roles in macrophage adhesion and migration. Wiskott–Aldrich syndrome protein (WASP; also known as WAS)-mediated actin polymerization is one of the key events initiating podosome formation. Nevertheless, membrane signals to trigger WASP activation at macrophage podosomes remain unclear. Here, we show that phosphatidylinositol (3,4,5)-trisphosphate [PI(3,4,5)P3] lipids are enriched at the podosome and stably recruit WASP rather than the WASP-5KE mutant. Phosphatidylinositol 4,5-bisphosphate 3-kinase catalytic subunit β (PIK3CB) is spatially located at the podosome core. Inhibition of PIK3CB and overexpression of phosphatase and tensin homolog (PTEN) impede F-actin polymerization of the podosome. PIK3CB activation is regulated by Abl1 and Src family kinases. At the podosome core, Src and Hck promote the phosphorylation of Tyr488 in the consensus Y-x-x-M motif of Abl1, which enables the association of phosphoinositide 3-kinase (PI3K) regulatory subunits. Knockdown of Abl1 rather than Abl2 suppresses the PI3K/Akt pathway, regardless of Src and Hck activities. Reintroduction of wild-type Abl1 rather than the Abl1-Y488F mutant rescues PI3KR1 recruitment and PI3K activation. When PIK3CB, Abl1 or Src/Hck is suppressed, macrophage podosome formation, matrix degradation and chemotactic migration are inhibited. Thus, Src/Hck-mediated phosphorylation of Abl1 Tyr488 triggers PIK3CB-dependent PI(3,4,5)P3 production and orchestrates the assembly and function of macrophage podosomes.

KEY WORDS: Abl, PI(3,4,5)P3 lipid, PI3K, Podosome

INTRODUCTION

The dynamic regulation of cell-matrix adhesion is important for maintaining cell motility and tissue reorganization (Legate et al., 2009; Parsons et al., 2010). Macrophages are migratory cells and natively assemble podosomes as the adhesion structure at the cell–matrix interface (Calle et al., 2006; Linder and Kopp, 2005). Each podosome is about 1-3 µm in diameter and exhibits an unique core/ring organization. Podosome cores contain dot-like F-actin assemblies with various actin regulating factors (Schachtner et al., 2013; Yu et al., 2013). Podosome rings are composed of integrin receptors and adhesion-related adaptor proteins (such as paxillin and vinculin) and encircle podosome cores. Podosome formation is vital for macrophage cells to perform matrix degradation and chemotactic migration through tissue compartments (El Azzouzi et al., 2016; Hoshino et al., 2013).

Dense and protrusive F-actin polymerization mediated by the actin-related protein 2/3 complex (Arp2/3) is one of the signature events during podosome formation (Albiges-Rizo et al., 2009; Cao et al., 2020). The polymerization of actin is initiated at the plasma membrane and is further extended into the cytosol (Zhang et al., 2019). Negatively charged lipids, such as phosphatidylinositol 4,5-bisphosphate [PI(4,5)P2] and phosphatidylinositol (3,4,5)-trisphosphate [PI(3,4,5)P3] are important membrane messengers and can activate various actin nucleation promoting factors (NPFs) (Campellone and Welch, 2010; Papayannopoulos et al., 2005). In particular, Wiskott–Aldrich syndrome protein (WASP; also known as WAS) is one of the NPFs found in the macrophage podosome (Linder et al., 1999). Upon binding to negatively charged lipids and Rho GTPases, WASP is released from auto-inhibitory conformation and recruits Arp2/3 to promote polymerization of the branched actin network (Abella et al., 2016; Pollard, 2007). PI(4,5)P2 lipids are mainly situated in the plasma membrane compartment and are observed in the concentration range of 5000-20,000 molecules/µm^2 (Balla, 2013; Falkenburger et al., 2010). PI(3,4,5)P3 lipids are a rare species of phosphatidylinositols and are produced by phosphoinositide 3-kinase (PI3K)-mediated phosphorylation of PI(4,5)P2 lipids (Bilanges et al., 2019; Fruman et al., 2017). PI(3,4,5)P3 lipids can then be dephosphorylated by inositol phosphatases and become PI(4,5)P2 or phosphatidylinositol (3,4)-bisphosphate [PI(3,4)P2] lipids. The amount of PI(3,4,5)P3 lipids is tightly regulated and only contributes about 2-5% of the amount of PI(4,5)P2 lipids (Falkenburger et al., 2010). The biogenesis of PI(3,4,5)P3 is crucial in many cell biological events, including Akt phosphorylation, localized actin polymerization and directional cell migration (Insall and Weiner, 2001; Manning and Toker, 2017).

Src family kinases are membrane-bound non-receptor tyrosine kinases that play important roles in cell adhesion and migration. In particular, blockage of Src family kinases, such as Src and hematopoietic-specific Hck, can impede podosome formation in macrophages (Cougoule et al., 2010; Linder et al., 2000). In cancer cells, Src-mediated phosphorylations of Tks5 and cortactin are known to promote the formation of invadopodia, which exhibit a similar ring/core organization as macrophage podosomes (Murphy and Courtneidge, 2011). Src family kinases can also phosphorylate Abl and activate various Abl-mediated signal transductions (Hantschel and Superti-Furga, 2004; Khatri et al., 2016). Specifically, Abl can recruit PI3K regulatory subunits (p85) via its Tyr488-phosphorylated YELM motif (the consensus Y-x-x-M motif, where x is any residue) (Jain et al., 1996; Songyang et al., 1993) or via intermediate effectors, such as Abi1 and CrkII (Dubielecka et al., 2010; Ren et al., 1994). A constitutively active Abl mutant (BCR-ABL, chimeric oncogene) can cause hyperactivation of the PI3K signaling cascade and uncontrolled cell proliferation (Hantschel and Superti-Furga, 2004).

School of Biomedical Sciences, Faculty of Medicine, University of Hong Kong, Hong Kong.

*Author for correspondence (chyu1@hku.hk)

C.-h.Y., 0000-0002-8821-8877

Handling Editor: Michael Way
Received 16 May 2019; Accepted 22 April 2020

Journal of Cell Science (2020) 133, jcs234385. doi:10.1242/jcs.234385

Macrophages often form multiple podosomes concurrently. Signals to trigger F-actin polymerization and depolymerization determine the lifetime of an individual podosome (usually 50-200 s). Spatiotemporal activations of the membrane-associated kinases PI3K, Abl and Src can serve as upstream signals to orchestrate lipid messenger-mediated NPF activation and F-actin polymerization. In this study, we reveal the signaling cascade of Src/Hck–Abl1–PIK3CB and PI(3,4,5)P3 biogenesis to regulate WASP activation and macrophage podosome formation.

RESULTS

PI(3,4,5)P3 lipids are specifically enriched at macrophage podosomes

Dynamic distribution of phosphatidylinositol lipids can be revealed using species-specific binding probes. GFP-tagged PH-GRP1, PH-PLCD1, PH-TAPP1, P4M-SidM and PX-p40 were transfected and used as lipid-binding probes to report the spatiotemporal distribution of PI(3,4,5)P3, PI(4,5)P2, PI(3,4)P2, phosphatidylinositol 4-phosphate (PI4P) and phosphatidylinositol 3-phosphate (PI3P). In RAW 264.7 macrophage cells, we found that PH-GRP1 was enriched at the F-actin core of the podosome (Fig. 1A,B; Movie 1). The intensity level of PH-GRP1 increased during the F-actin assembly phase of podosomes (Fig. 1C,D). In the podosome disassembly phase, the intensity level of PH-GRP1 also decreased in a similar fashion as F-actin. In agreement with PH-GRP1 enrichment, PH-BTK, another PI(3,4,5)P3 binding probe, was also concentrated at the podosome core (Fig. S1A,B). On the other hand, PH-PLCD1, PH-TAPP1, P4M-SidM and PX-p40 did not show distinct colocalization with podosomes (Fig. 1E-H; Fig. S1C-J). It appears that PI(3,4,5)P3 lipids are locally produced during the process of podosome formation.

The lipid-binding motif of WASP determines its enrichment at the podosome

GFP-WASP colocalized with F-actin at the podosome core (Fig. 1I; Movie 2). Other phosphoinositide-associated actin polymerization factors, such as Tks5 and WASF2, were not distinctly enriched at the podosome (Fig. S1K,L). When key lysine residues in the lipid-binding domain of WASP were mutated to glutamic acids (WASP-5KE; K226E, K230E, K231E, K232E and K235E) (Rohatgi et al., 2000), GFP-WASP-5KE showed poor enrichment at the podosome (Fig. 1J; Movie 3). During each cycle of podosome formation, changes in the intensity of wild-type WASP were synchronized with those of F-actin (Fig. 1K,L). However, the intensity of WASP-5KE exhibited disorganized fluctuations and low degrees of synchronization with that of F-actin (Fig. 1M,N). These results suggest that positively charged residues in the lipid-binding domain of WASP play an essential role in the stable recruitment of WASP to the podosome.

PIK3CB is enriched at the podosome core

Class I PI3Ks are key enzymes in production of PI(3,4,5)P3 lipids in the plasma membrane. We employed reverse transcription quantitative polymerase chain reaction (RT-qPCR) to evaluate the expression level of various PI3K catalytic subunits in RAW 264.7 macrophage cells. Although all four isoforms of class I PI3K catalytic subunits were detected, the β-subunit (PIK3CB) exhibited the highest expression level (Fig. 2A). In addition, EGFP-PIK3CB was enriched at the podosome core (Fig. 2B,C; Movie 4). Intensity fluctuations of PIK3CB were also synchronized with those of F-actin (Fig. 2D; Fig. S2A,B). Other class I PI3K isoforms, including PIK3CA, PIK3CD and PIK3CG (α-, δ- and γ-subunits, respectively) were largely diffusive and exhibited weak associations with podosomes (Fig. S2C-E).

Knockdown of PIK3CB blocks the podosome formation

When PIK3CB expression was suppressed by siRNA, the percentage of cells forming podosomes was significantly reduced in comparison with the si-Scramble control (Fig. 2E,F). Macrophages transfected with si-Scramble showed distinct dot-like F-actin in podosome cores that was surrounded by adhesion adaptor protein paxillin (Fig. 2G,H). Knockdown of PIK3CB resulted in loss of the dot-like assembly of F-actin and the ring assembly of paxillin (Fig. 2I). Overall F-actin intensities revealed by phalloidin staining were also reduced (Fig. 2J). Notably, expressions of PIK3CG and PIK3CD remained unchanged, but the level of PIK3CA expression increased when PIK3CB was knocked down (Fig. S3A). Nevertheless, knockdown of PIK3CB rather than PIK3CA reduced the levels of Akt phosphorylated at Ser473 (pS473-Akt) (Fig. S3B,C). Because the level of pS473-Akt is one of the major indicators of PI(3,4,5)P3-mediated signal transduction, it appears that PIK3CB is the key enzyme in producing PI(3,4,5)P3 lipids and supporting macrophage podosome formation.

PIK3CB inhibition triggers the dissociation of WASP and disassembly of F-actin

Inhibitors of PIK3CB (TGX-221, 500 nM) and pan-PI3K (LY294002, 1 μM; Wortmannin, 200 nM) blocked the dot-like assembly of F-actin in macrophage podosomes (Fig. S4A,B). However, F-actin assemblies at the podosome were not suppressed when PIK3CD inhibitor (CAL-101,100 nM) and PIK3CA inhibitor (A66, 100 nM) were introduced. Treatment with TGX-221 caused the dissociation of PH-GRP1, WASP and Arp3 from podosomes, and the dot-like assembly of F-actin at the pre-existing podosome gradually faded away (Fig. 2K-M; Movies 5-7). After 30 min of TGX-221 treatment, PH-GRP1, WASP and Arp3 were largely diffusive and *de novo* F-actin polymerization was largely suppressed.

PTEN negatively regulates podosome formation

Phosphatase and tensin homolog (PTEN) is a 3′-inositol phosphatase that can dephosphorylate PI(3,4,5)P3 lipids and is an antagonist of PI3K signaling. GFP-tagged PTEN was found at the podosome core (Fig. 3A,B). The recruitment of PTEN was synchronized with the F-actin assembly at the podosome core (Fig. 3C; Movie 8). Overexpression of a constitutively active PTEN-A4 mutant (Vazquez et al., 2000) resulted in a decrease in the percentage of cells forming podosomes in comparison with the empty vector control (Fig. 3D,E).

PI3K regulatory subunit PIK3R1 and Tyr488-phosphorylated Abl colocalize at the podosome core

GFP-tagged PI3K regulatory subunit PIK3R1 and Abl1 were both located at the podosome core (Fig. 4A-F). During podosome formation, recruitment of PIK3R1 and Abl1 to the podosome was also synchronized with the assembly of F-actin (Fig. 4C,F; Movies 9,10). In addition, Tyr488-phosphorylated Abl (pY488-Abl), which enables direct binding to PIK3R1 (p85 alpha) (Jain et al., 1996; Yuan et al., 1997), was observed at the podosome core (Fig. 4G,H). Src family kinases are among the key factors in Abl phosphorylation. Tyr416-phosphorylated Src (pY416-Src), a specific indicator of Src family kinase activation, was also found at the podosome core (Fig. 4I,J). Other potential adaptor proteins between PIK3R1 and Abl, such as Abi1 (Abl interactor 1) and CrkII, were associated with the podosome ring and were absent from the podosome core (Fig. S5A,B).

Journal of Cell Science (2020) 133, jcs234385. doi:10.1242/jcs.234385

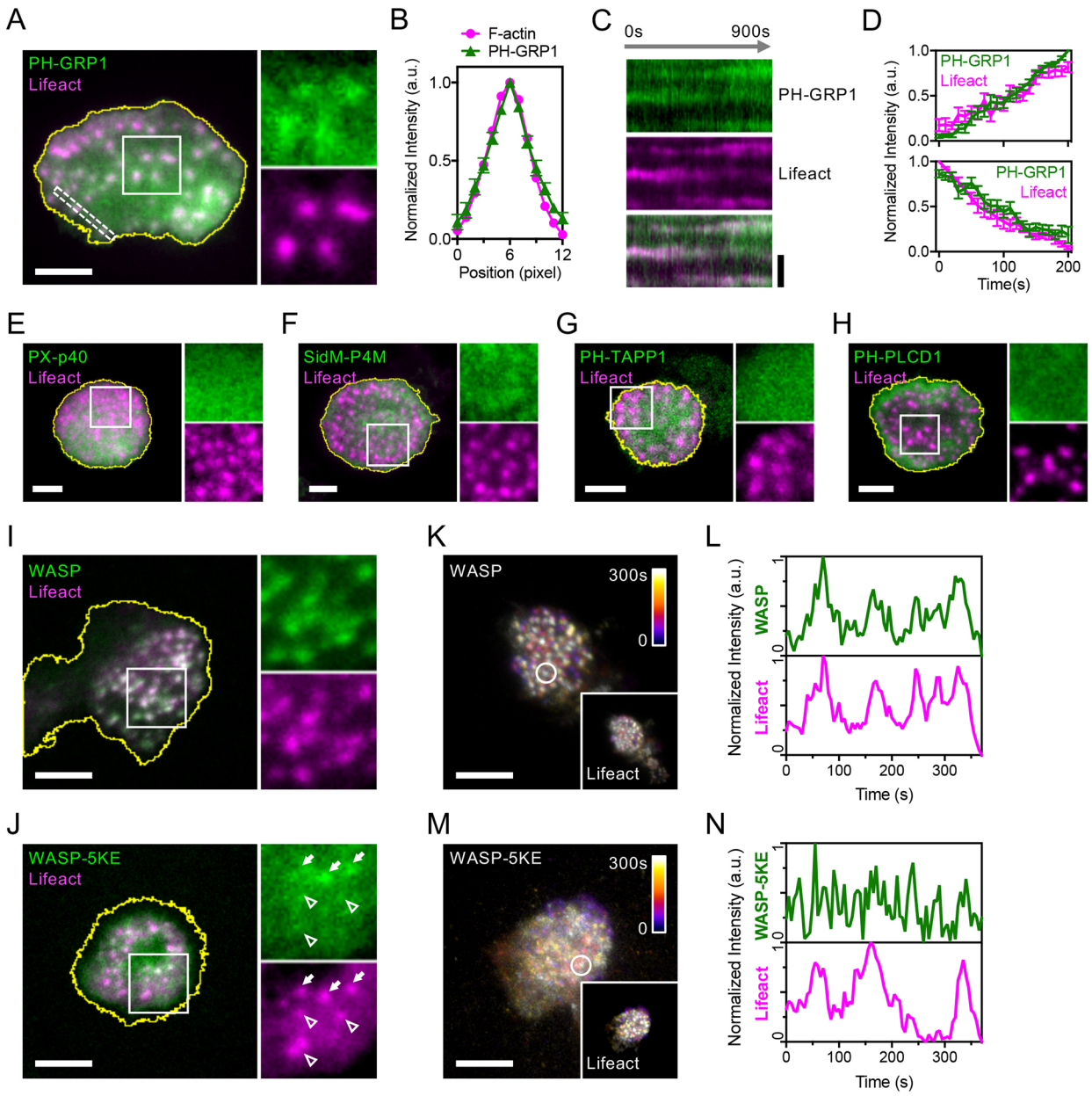

Fig. 1. PI(3,4,5)P3-dependent WASP enrichment at the macrophage podosome. (A) EGFP-PH-GRP1 [PI(3,4,5)P3 lipid probe] colocalizes with F-actin marker lifeact-EBFP2 at the podosome core in RAW 264.7 macrophages. Insets show magnifications of the boxed region (5×5 μm^2). See Movie 1. (B) Intensity profiles of PH-GRP1 and lifeact exhibit similar distributions across the podosome (12 podosomes in 3 cells). (C) Kymograph along the dashed box in A. The enrichments of PH-GRP1 and lifeact show a synchronized pattern during podosome formation. (D) Time-dependent intensity fluctuations of PH-GRP1 and lifeact. When the podosome start to form, intensities of PH-GRP1 and lifeact both increase progressively. As podosomes start to disassemble, intensities of PH-GRP1 and lifeact both decrease (10 podosomes each). (E-H) PX-p40-EGFP (PI3P probe), EGFP-P4M-SidM (PI4P probe), PH-TAPP1-EGFP [PI(3,4)P2 probe] and PH-PLCD1-EGFP [PI(4,5)P2 probe] do not exhibit distinct colocalization with lifeact-mRuby at the podosome core. Insets show magnifications of the boxed region (5×5 μm^2). (I,J) GFP-WASP colocalizes with lifeact-EBFP2. GFP-WASP-5KE shows a limited degree of colocalization with lifeact (arrows). Many lifeact-marked podosomes lack WASP-5KE (empty arrowheads). Insets show magnifications of the boxed region (5×5 μm^2). (K) Time-projected pseudocolor images of GFP-WASP (300 s). Inset: time-projected pseudocolor images of lifeact-EBFP2. WASP is consistently enriched at the lifeact-marked podosome. (L) Normalized intensities of WASP and lifeact measured in the circled ROI in K. WASP and lifeact exhibit synchronized intensity fluctuations during each cycle of podosome formation. See Movie 2. (M) Time-projected pseudocolor images of GFP-WASP-5KE (300 s). Inset: time-projected pseudocolor images of lifeact-EBFP2. WASP-5KE exhibits a diffusive pattern and is not consistently enriched at the lifeact-marked podosome. See Movie 3. (N) Normalized intensities of WASP-5KE and lifeact measured in the circled ROI in M. Intensity fluctuations of WASP-5KE are largely stochastic and exhibit a low level of synchronization with those of lifeact. The experiments shown contain at least three independent biological repeats. Graphs give mean±s.e.m. Scale bars: 5 μm.

Knockdown of Abl1 suppresses PI3K activity and podosome formation

When expression of Abl1 or Abl2 was suppressed by siRNA, only si-Abl1 resulted in significant reduction in pS473-Akt levels compared with si-Scramble control (Fig. 5A). The levels of pY416-Src remained unchanged, regardless of Abl1 or Abl2 knockdown. Knockdown of Abl1 also reduced the percentage of cells forming podosomes compared with si-Scramble control

Journal of Cell Science (2020) 133, jcs234385. doi:10.1242/jcs.234385

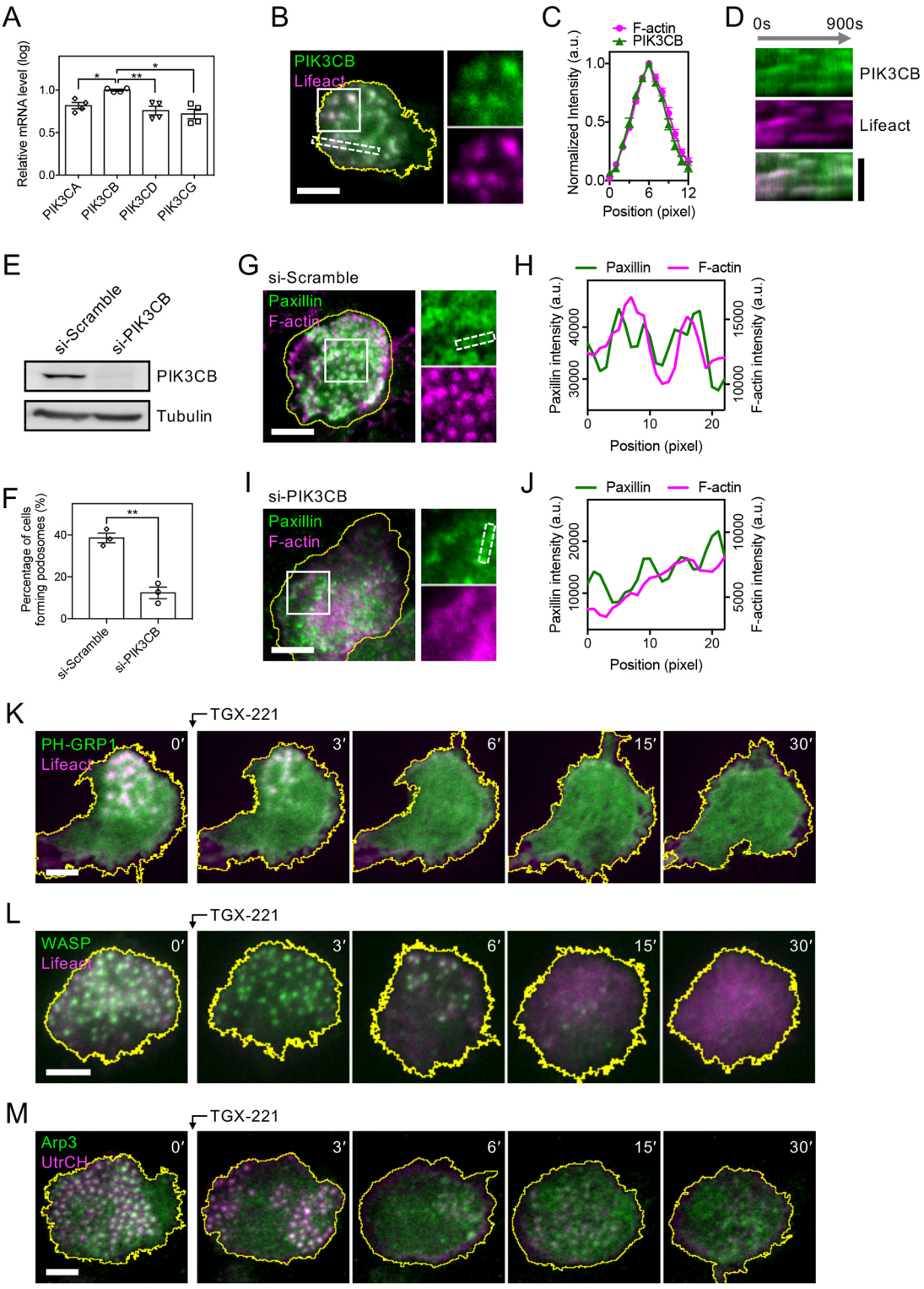

Fig. 2. See next page for legend.

(Fig. 5B-D). Reintroduction of wild-type Abl1, rather than non-phosphorylatable Abl1-Y488F mutant, led to the rescue of pS473-Akt levels and podosome formation. Likewise, reintroduced wild-type Abl1 (instead of Abl1-Y488F mutant) colocalized with PIK3R1 and the dot-like assembly of F-actin (Fig. S5C,D).

Src and Hck regulate Tyr488-phosphorylation of Abl and PI3K activity

When Src and Hck were both knocked down, the levels of pS473-Akt were significantly reduced in comparison with the si-Scramble control and single knockdown of Src or Hck (Fig. 5E-G). Dual knockdown of Src and Hck also reduced the levels of

Journal of Cell Science (2020) 133, jcs234385. doi:10.1242/jcs.234385

Fig. 2. PIK3CB is an essential component of macrophage podosome. (A) RT-qPCR analyses of class I PI3Ks in RAW 264.7 macrophages. PIK3CB exhibits the highest expression. One-way ANOVA with Dunnet's test is applied. Statistical information is in Table S1A. (B) EGFP-PIK3CB colocalizes with F-actin marker lifeact-mRuby at the podosome core. Insets show magnifications of the boxed region (5×5 μm^2). See Movie 4. (C) Intensity profiles of PIK3CB and lifeact show similar distributions across the podosome (12 podosomes in 3 cells). (D) Kymograph along the dashed box in B. PIK3CB and lifeact exhibit synchronized enrichments. (E) Western blots confirm the knockdown of PIK3CB by siRNA. (F) Knockdown of PIK3CB results in the reduction of podosome-forming cells. Unpaired two-tailed Student's *t*-test is applied. Statistical information is in Table S1B. (G) In si-Scramble transfected cells, each podosome can be identified with a distinct F-actin core surrounded by a paxillin ring. F-actin and paxillin are labeled with CF594-phalloidin and AF488-anti-paxillin antibody, respectively. Insets show magnifications of the boxed region (5×5 μm^2). (H) Intensity profiles of paxillin and F-actin along the dashed box in G. Each peak of F-actin is enclosed by two peaks of paxillin. (I) There are no distinct core and ring organizations in si-PIK3CB-transfected cells. Insets show magnifications of boxed region (5×5 μm^2). (J) Intensity profiles of paxillin and F-actin along the dashed box in I. Under the same staining condition as for H, there are no apparent F-actin peaks observed among paxillin-labeled adhesions and the intensities of F-actin and paxillin are reduced. (K-M) EGFP-PH-GRP1, EGFP-WASP and mCherry-Arp3 are enriched at F-actin of the podosome core marked by lifeact-EBFP2, lifeact-mRuby and GFP-UtrCH, respectively. After TGX-221 is introduced, PH-GRP1, WASP and Arp3 become disorganized and F-actin start to depolymerize. Macrophage podosomes disassemble within 30 min. See Movies 5-7. The experiments shown contain at least three independent biological repeats. Bar charts show mean±s.e.m. **P*<0.0332, ***P*<0.0021. Scale bars: 5 μm.

pY488-Abl and reduced the percentage of cells forming podosomes (Fig. 5H-J). Likewise, chemical inhibition of Src (PP2, 10 μM) and Abl (Imatinib, 10 μM) blocked podosome formation, and the distribution of PIK3R1, Abl1 and PH-GRP1 in macrophages became largely diffusive (Fig. S6A-J). Although each knockdown of Abl1 or Src/Hck suppressed the levels of pS473-Akt, the levels of pY488-Abl and pY416-Src remained unchanged when PIK3CB was knocked down (Fig. 5K).

Inhibition of Src/Hck–Abl1–PIK3CB signal pathway suppresses matrix degradation and macrophage chemotactic migration

Macrophages utilize podosomes to degrade extracellular matrices and to migrate through tissues. When PIK3CB, Abl1 or Src/Hck was knocked down, the degraded areas of gelatin matrices were significantly reduced compared with si-Scramble control (Fig. 6A,B). Using serum-containing medium as the chemoattractant, macrophage migration through the transwell chamber was attenuated when PIK3CB, Abl1 or Src/Hck was knocked down (Fig. 6C,D). It appears that the signal pathway involving Src/Hck, Abl1 and PIK3CB plays an essential role in maintaining the physiological functions of macrophage podosomes.

DISCUSSION

Macrophages form podosomes to maintain cell adhesion and motility. Each podosome has a lifetime of 50-200 s and contains a prominent dot-like F-actin assembly surrounded by an integrin-mediated adhesion ring. WASP is the key NPF at the plasma membrane, enabling Arp2/3-mediated actin polymerization of the podosome. Here, we investigate the spatiotemporal membrane signals that trigger WASP activation. We examined the distributions of various phosphatidylinositol species and found that PI(3,4,5)P3 lipids are distinctly enriched at the podosome. The WASP-5KE mutant, in which lysine residues in the lipid-binding region of WASP are changed to glutamic acids, loses organized recruitment to the podosome. In addition, we found that PIK3CB is enriched at the podosome core and locally produces PI(3,4,5)P3 lipids. Various

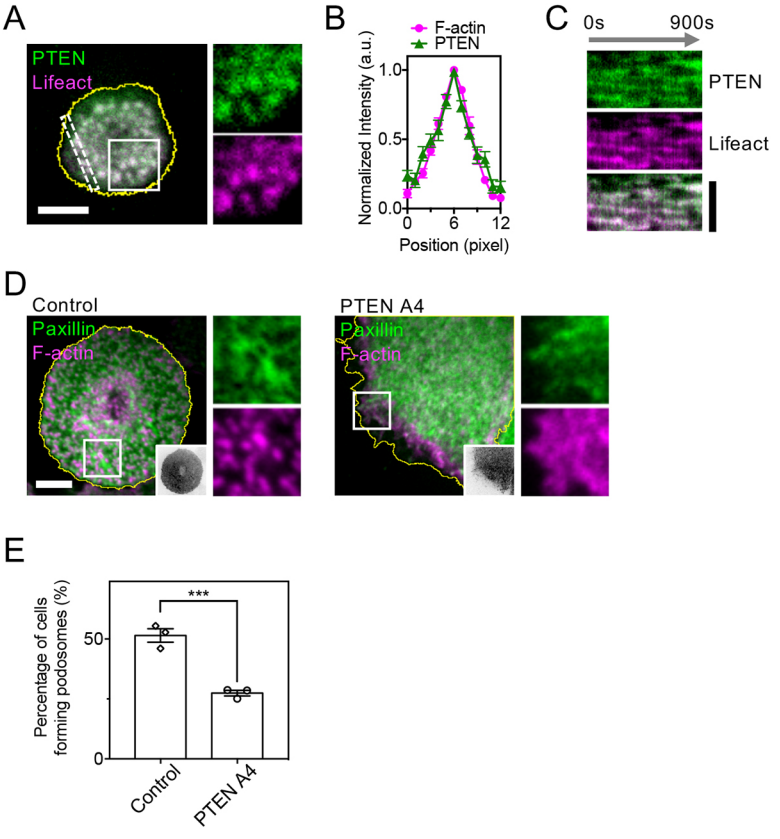

Fig. 3. PTEN is a negative regulator of macrophage podosome. (A) EGFP-PTEN colocalizes with F-actin marker lifeact-mRuby at the podosome core in RAW 264.7 macrophages. Insets show magnifications of the boxed region (5×5 μm^2). See Movie 8. (B) Intensity profiles of PTEN lifeact exhibit similar distributions across the podosome (12 podosomes in 3 cells). (C) Kymograph along the dashed box in A. PTEN and lifeact exhibit synchronized enrichments during podosome formation. (D) Compared with EGFP control, overexpression of constitutively active EGFP-PTEN-A4 mutant suppresses podosome formation. Podosome core and ring are visualized using CF680-phalloidin and RFP-paxillin, respectively. Inverted images represent EGFP empty vector and EGFP-PTEN-A4 expressed in each of the cells. Insets show magnifications of the boxed region (5×5 μm^2). (E) Percentage of cells that form podosomes after the introduction of empty vector control or PTEN-A4 mutant. Unpaired two-tailed Student's t-test is applied. Statistical information is in Table S1C. Experiments shown were performed with at least three independent biological repeats. Bar charts show mean±s.e.m. ****P*<0.0002. Scale bars: 5 μm.

Journal of Cell Science (2020) 133, jcs234385. doi:10.1242/jcs.234385

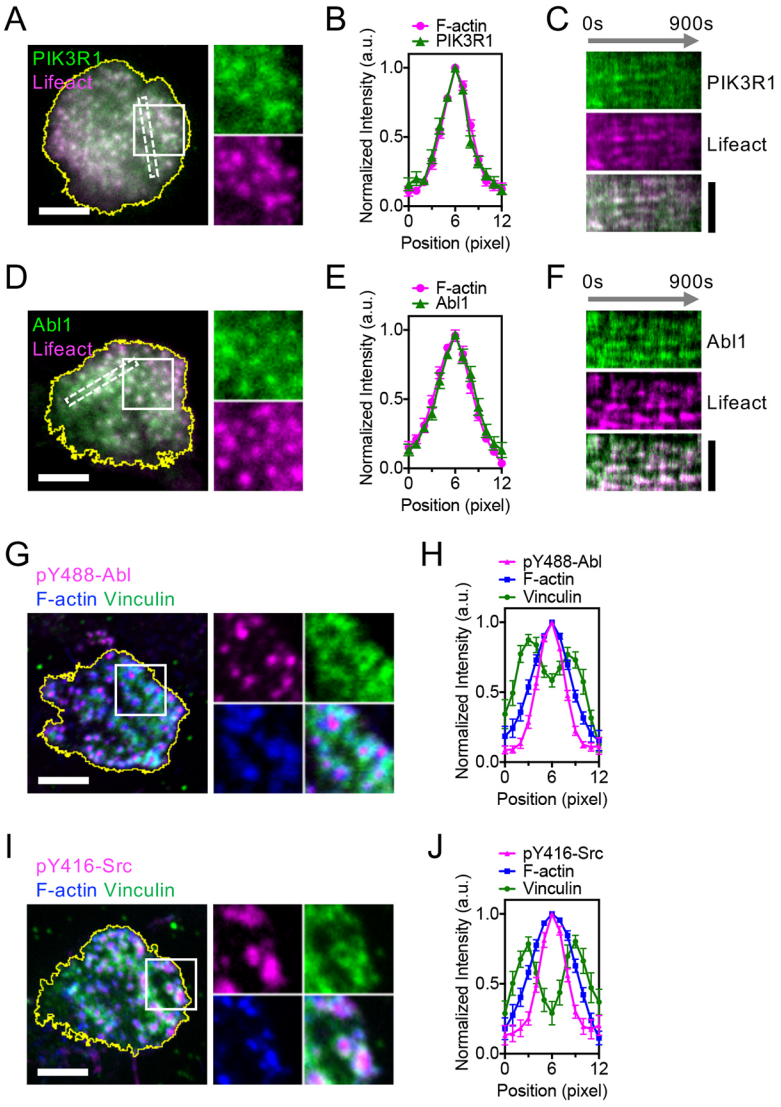

Fig. 4. PIK3R1 and Tyr488-phosphorylated Abl1 are enriched at the podosome core. (A) EGFP-PIK3R1 (regulatory subunit of PI3K) colocalizes with F-actin marker lifeact-mRuby at the podosome core in RAW 264.7 macrophages. Insets show magnifications of boxed region (5×5 μm^2). See Movie 9. (B) Intensity profiles of PIK3R1 and lifeact exhibit similar distributions across the podosome (12 podosomes in 3 cells). (C) Kymograph along the dashed box in A. PIK3R1 and lifeact show synchronized enrichments. (D) Abl1-EGFP colocalizes with lifeact-mRuby at the podosome core. Insets show magnifications of the boxed region (5×5 μm^2). See Movie 10. (E) Intensity profiles of Abl1 and lifeact show similar distributions across the podosome (12 podosomes in 3 cells). (F) Kymograph along the dashed box in D. The enrichments of Abl1 and lifeact exhibit a synchronized pattern during the podosome formation. (G) Abl1 phosphorylation at Y488 is detected by phospho-specific antibody and is found at the podosome core. F-actin and the podosome ring are labeled by CF680R-phalloidin and AF594-anti-vinculin antibody, respectively. Insets show magnifications of boxed region (5×5 μm^2). (H) Intensity profiles of pY488-Abl1, F-actin and vinculin across the podosome (12 podosomes in 3 cells). F-actin and pY488-Abl1 share the same peak position at the podosome core and are enclosed by two peaks of vinculin. (I) Src phosphorylation at Y416 is detected by phospho-specific antibody and is found at the podosome core. F-actin and the podosome ring are labeled by CF680R-phalloidin and AF594-anti-vinculin antibody, respectively. Insets show magnifications of the boxed region (5×5 μm^2). (J) Intensity profiles of pY416-Src, F-actin and vinculin across the podosome (12 podosomes in 3 cells). F-actin and pY416-Src have the same peak position at the podosome core and are enclosed by two peaks of vinculin. The experiments shown contain at least three independent biological repeats. Graphs give mean±s.e.m. Scale bars: 5 μm.

approaches that impede PI(3,4,5)P3 production, including knockdown and chemical inhibition of PIK3CB and overexpression of constitutively active inositol phosphatase PTEN-A4, lead to the blockage of dot-like F-actin polymerization and suppression of podosome formation.

Lipid signals to activate N-WASP, another NPF homologous to WASP, have been investigated (Papayannopoulos et al., 2005; Rohatgi et al., 2000). Both PI(4,5)P2 and PI(3,4,5)P3 lipids can bind to the basic region of N-WASP with similar affinities (dissociation constants 1.1 and 2.4 μM, respectively) and release N-WASP from the autoinhibited conformation. As PI(4,5)P2 lipids are not locally enriched at the podosome, our results suggest that the level of PI(3,4,5)P3 lipid is the key membrane signal for WASP recruitment. The local enrichment of PI(3,4,5)P3 lipids may also promote recruitment of guanine nucleotide exchange factors of Rho GTPases, which further support the full activation of WASP (Campellone and Welch, 2010). Our results also indicate that WASF2, another PI(3,4,5)P3-associated NPF, is not enriched at the macrophage podosome. The recruitment and activation of WASF2 may require additional factors (Ismail et al., 2009).

Notably, the involvement of PI4P lipids has also been reported in macrophage podosomes (El Azzouzi et al., 2016). Because membrane-bound matrix metalloproteinase MT1-MMP in the PI4P-rich Golgi is actively delivered to the podosome, the physical contact and membrane fusion between Golgi and the plasma membrane may contribute to the local enrichment of PI4P lipids. Nevertheless, kinases and phosphatases responsible for PI4P production at the podosome remain to be investigated.

Spatiotemporal factors that determine the distribution of the PI3K regulatory subunit can control PI3K activity. We found that PIK3R1, pY488-Abl and activated Src family kinases are all distinctly located at the podosome core. Knockdown of Abl1 rather than Abl2 attenuates PI3K activation (pS473-Akt level) and suppresses macrophage podosome formation. The Abl1-Y488F mutant, in which Tyr488 in the consensus Y-x-x-M motif for PIK3R1 binding is mutated to phenylalanine, cannot rescue PI3K activation and fails to restore podosome formation. Likewise, when two Src family kinases (Src and Hck) are both knocked down, the levels of pY488-Abl and pS473-Akt are reduced and podosome formation is suppressed. Examining their impacts on the physiological function of macrophage podosomes, we found that single knockdown of PIK3CB or Abl1 and dual knockdown of Src/Hck lead to defects in matrix degradation and chemotactic migration.

Journal of Cell Science (2020) 133, jcs234385. doi:10.1242/jcs.234385

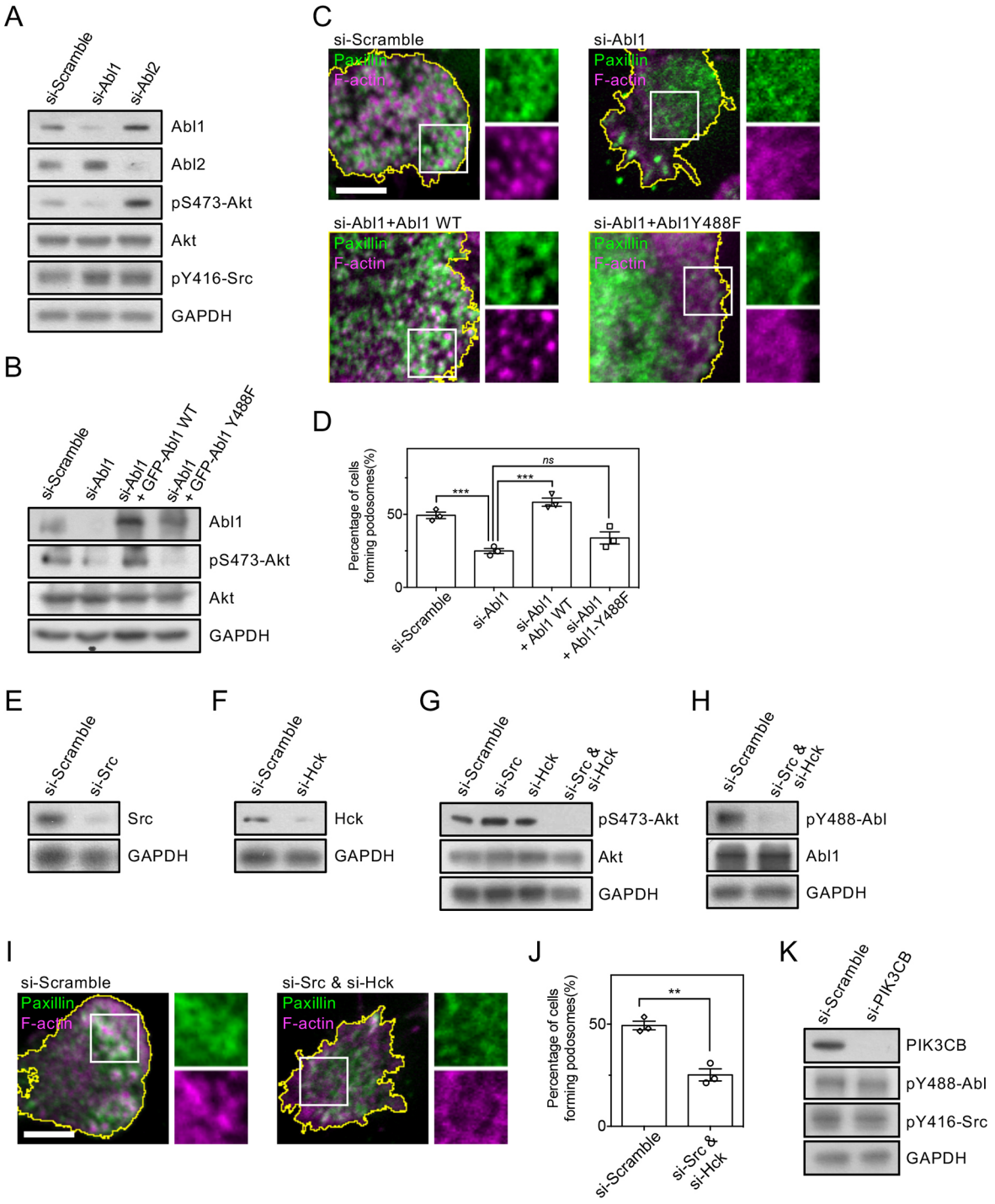

Fig. 5. Tyr488 phosphorylation of Abl1 by Src and Hck is vital for macrophage podosome formation. (A) Western blot analyses show that the levels of pS473-Akt reduce when si-Abl1 instead of si-Abl2 is introduced to RAW 264.7 macrophages. The levels pf pY416-Src remain unchanged. (B) Western blot analyses indicate that rescue with wild-type Abl1 rather than Abl1-Y488F restores the levels of pS473-Akt. (C) Knockdown of Abl1 blocks podosome formation. Rescue with wild-type Abl1 rather than Abl1-Y488F restores assembly of the podosome core (F-actin, phalloidin staining) and ring (paxillin antibody staining). Insets show magnifications of the boxed region (5×5 μm^2). (D) Percentage of cells that form podosomes after knockdown and rescue as indicated. One-way ANOVA with Dunnett's test is applied. Statistical information is in Table S1D. (E,F) Western blots confirm the knockdown of Src and Hck, respectively. (G) Western blot analyses show that the levels of pS473-Akt reduce when both si-Src and si-Hck are introduced. Single knockdown of Src or Hck fails to suppress the Ser473 phosphorylation of Akt. (H) Western blot analyses show that dual knockdown of Src and Hck reduces the levels of pY488-Abl. (I) Compared with si-Scramble control, dual knockdown of Src and Hck blocks assembly of the podosome core (F-actin, phalloidin staining) and ring (paxillin antibody staining). Insets show magnifications of the boxed region (5×5 μm^2). (J) Percentage of cells that form podosomes after si-Scramble or dual knockdown of Src and Hck. Unpaired two-tailed Student's *t*-test is applied. Statistical information is in Table S1E. (K) Western blot analyses indicate that knockdown of PI3KCB does not suppress the levels of pY488-Abl and pY416-Src. The experiments shown contain at least three independent biological repeats. Bar charts show mean±s.e.m. ns $P>0.1234$, $^{**}P<0.0021$, $^{***}P<0.0002$. Scale bars: 5 μm.

Journal of Cell Science (2020) 133, jcs234385. doi:10.1242/jcs.234385

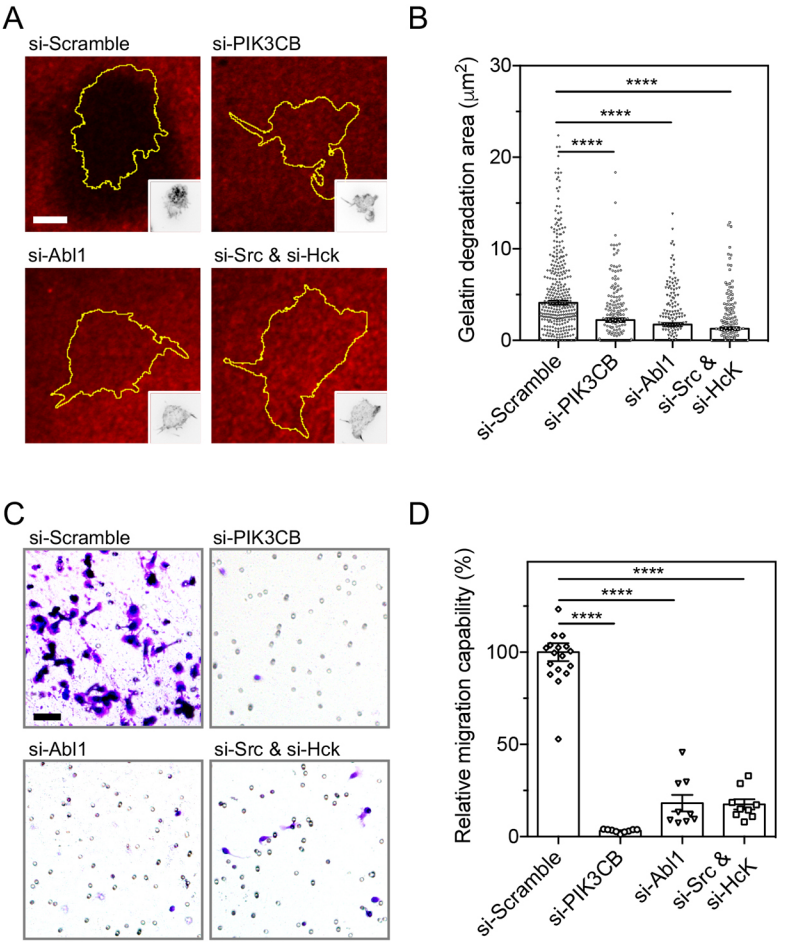

Fig. 6. Src-Abl-PI3K signaling regulates gelatin degradation and transwell migration of macrophage cells. (A) RAW 264.7 macrophages actively degrade Cy3-labeled gelatin substrata. Each knockdown of PIK3CB and Abl1 and dual knockdown of Src and Hck reduce the areas of degraded gelatin substrata in comparison with si-Scramble control. Inset: inverted images represent CF680R-phalloidin staining of F-actin in each of the cells. (B) Areas of degraded gelatin substrata after si-Scramble and each knockdown as indicated. One-way ANOVA with Dunnett's test is applied. Statistical information is in Table S1F. (C) Using the serum-containing medium as the chemoattractant, macrophages migrate through the transwell chamber and are identified with crystal violet staining. In comparison with si-Scramble control, the number of migrated cells becomes reduced with single knockdown of PIK3CB or Abl1 and dual knockdown of Src and Hck. (D) Migration capability of the indicated knockdown cells relative to migration of si-Scramble control cells. One-way ANOVA with Dunnett's test is applied. Statistical information is in Table S1G. The experiments shown contain at least three independent biological repeats. Bar charts represent mean ±s.e.m. ****P<0.0001. Scale bars: 5 µm (A), 50 µm (C).

Although PIK3CB, Abl1 and Src/Hck all play crucial roles in macrophage podosome, we further determined the causality among them. In particular, we found that Abl1 knockdown suppresses the levels of pS473-Akt but the levels of pY416-Src remain unchanged. This suggests that activated Src family kinases are not sufficient to support PIK3CB activation and podosome formation. Likewise, knockdown of PIK3CB does not affect the levels of pY488-Abl and pY416-Src. This implies that PI(3,4,5)P3 biogenesis plays an indispensable role in podosome formation, irrespective of the activation of Src family kinases. Together, these observations indicate that Src and Hck serve as upstream regulators to initiate Abl1-dependent signal transductions at the macrophage podosome (Fig. 7). Tyr488 phosphorylation of Abl1 acts as the crucial factor to support PIK3CB activation. PIK3CB gives rise to PI(3,4,5)P3 lipid production, which triggers WASP-mediated F-actin polymerization and promotes podosome formation.

Activation of Src family kinases at cell–matrix adhesions have been well documented (Mitra and Schlaepfer, 2006). Although autophosphorylated focal adhesion kinase (FAK) can stabilize activated Src at integrin-mediated adhesions, FAK mainly resides at the podosome ring instead of the podosome core (Duong and Rodan, 2000; Yu et al., 2013). Therefore, the podosome core-specific enrichment of activated Src might contribute from the interaction with other components. CD44, the hyaluronan receptor, is a single-pass transmembrane protein and is enriched at the podosome core (Chabadel et al., 2007). The cytoplasmic tail of CD44 can bind to Src with high affinity (dissociation constant about 2 nM) (Bourguignon et al., 2001). Knockdown of CD44 can reduce Src activity and suppress invadopodia formation (Zhao et al., 2016). The functional role of CD44 in PI3K activation at the macrophage podosome remains to be studied.

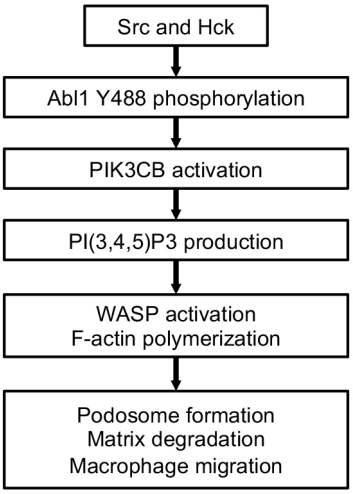

Fig. 7. Src and Hck serve as upstream regulators, initiating Abl1-dependent signal transductions at the macrophage podosome. The signal axis of Src/Hck–Abl1–PIK3CB promotes PI(3,4,5)P3 production, WASP-mediated F-actin polymerization and podosome formation in macrophage cells.

Journal of Cell Science (2020) 133, jcs234385. doi:10.1242/jcs.234385

Macrophage podosomes and cancer invadopodia are both integrin-mediated adhesions and share many similarities. Nevertheless, the signal transductions of podosomes and invadopodia can be distinctly different. For example, Abl2 and PIK3CA have been investigated in invadopodia-forming cancer cells (Fruman et al., 2017; Gil-Henn et al., 2013). However, we found that Abl1 and PIK3CB, instead of Abl2 and PIK3CA, are key factors in the regulation of macrophage podosomes. Likewise, PI(3,4)P2 lipids and the 5′-inositol phosphatase SHIP2 are particularly enriched at invadopodia (Sharma et al., 2013). PI(3,4)P2-selective effectors Tks5 and lamellipodin are involved in the formation and stabilization of invadopodia (Carmona et al., 2016; Oikawa et al., 2008). We found that PI(3,4)P2 lipids and Tks5 lack specific enrichment at the macrophage podosome. Although PI(3,4,5)P3 lipids in the plasma membrane are often rare and short-lived, spatiotemporal activation of PI3K and inositol phosphatase provides a closely controlled mechanism for regulating PI(3,4,5)P3-dependent events at the right time and the right place. In general, a comprehensive understanding of the diffusive characteristics and the rapid turnover of phosphatidylinositol signaling has profound implications for a wide range of cellular processes, including pattern formation, GTPase regulation and cell motility.

MATERIALS AND METHODS

Cell culture

The RAW264.7 macrophage cell line was obtained from American Type Culture Collection (TIB-71) and tested negative for contamination. Macrophage cells were cultured in Dulbecco's modified Eagle's medium (DMEM, high glucose, supplemented with 11% FBS) in a 37°C incubator with 5% CO_2.

RT-qPCR gene expression analysis

Total RNA was isolated using RNeasy Plus Mini Kit in accordance with the manufacturer's instructions (74134, Qiagen). RNA purity was measured using a NanoDrop2000c spectrophotometer (Thermo Fisher Scientific). Template cDNA was synthesized using SuperScript ll reverse transcriptase and Oligo $(dT)_{12\text{-}18}$ primer (18064014 and 18418012, Thermo Fisher Scientific). Quantitative PCR (qPCR) was performed using ChamQ SYBR color qPCR master mix (Vazyme, Q411) in MyiQ2 Real-Time PCR Detection System (Bio-Rad). Sequences of qPCR primers can be found in Table S2.

Plasmid

The following plasmids were obtained from Addgene: PX-p40-EYFP (19010) (Kanai et al., 2001), EGFP-P4M-SidM (51469) (Hammond et al., 2014), PH-PLCD-EGFP (51407) and BTK-GFP (51463) (Várnai and Balla, 1998), Lifeact (54674 and 54559) (Lam et al., 2012), GFP-UtrCH (26737) (Burkel et al., 2007), mCherry-Arp3 (27682) (Taylor et al., 2011), GFP-Abi1 (74905) (Innocenti et al., 2004), GFP-CrkII (50730), GFP-PTEN and GFP PTEN A4 (10759 and 10760) (Vazquez et al., 2000), and pCS DEST (13071 and 13075) (Villefranc et al., 2007). EGFP-WASP was a gift from Gareth E. Jones (King's College London). WASP-5KE mutant (K226E, K230E, K231E, K232E and K235E) was generated by PCR. RFP-Paxillin and Abl1-EGFP (human isoform b; long isoform) were gifts from Michael P. Sheetz (National University of Singapore). Abl1-Y488F mutant was generated by PCR and then subcloned into pLenti-based lentiviral vectors. Primer sequences to generate the mutants can be found in Table S3. EGFP-GRP1-PH was a gift from Guillaume Halet (Université de Rennes 1). TAPP1-PH-EGFP was a gift from Aaron Marshall (University of Manitoba). Tks5-EGFP was a gift from Min Wu (National University of Singapore). mEmerald-WAVE2-N-18 was a gift from Pakorn Kanchanawong (National University of Singapore). EGFP-PIK3CA (HsCD00036110) and EGFP-PIK3CB (HsCD00036098) were obtained from PlasmID Repository, Harvard Medical School. pENTR223-PIK3CD (HsCD00516484), pDNR-Dual-PIK3CG (HsCD00005739), and pENTR223-PIK3R1 (HsCD00288186) were obtained from DNASU Plasmid Repository, Arizona State University and were subcloned into Gateway Destination vectors, pLenti-based lentiviral vectors or pEGFP-based vectors.

Transfection

Transfections of non-lentiviral plasmids were achieved by electroporation (Neon transfection system, Thermo Fisher Scientific). Usually, 1 µg of each plasmid was introduced. After electroporation, transfected cells were cultured for 36-48 h before being used for experiments. A lentiviral transfection system was employed to achieve the knockdown-rescue experiment. HEK 293T cells in a T-25 flask were transfected with lentiviral expression constructs together with packaging plasmids psPAX2 and pMD2.G via PolyJet (SignaGen Laboratories). After 48-72 h, the supernatant with lentiviral particles was collected and filtered through a 0.22 µm filter. A mixture of viral supernatant (1 ml) and polybrene (10 µg/ml; TR-1003, Sigma) was then introduced to macrophage culture. Infected cells were cultured for at least 48 h before being used for experiments.

siRNA and chemical inhibition

siPIK3CB (SR421863), siPIK3CA (SR421939), siAbl1 (SR422207), siAbl2 (SR421985), siHck (SR416688) and scramble siRNAs were obtained from Origene. siSrc (D-040877-01-0002) was purchased from Dharmacon. siRNA sequences can be found in Table S4. After siRNA transfection, cells were cultured for 72 h before being used for experiments. Small molecular inhibitors TGX-221 (S1169), CAL-101 (S2226), A66 (S2636), LY294002 (S1105), wortmannin (S2758), PP2 (S7008) and Imatinib (S2475) were obtained from Selleckchem. Chemicals were dissolved in DMSO (Sigma Aldrich). Cells were treated with the indicated inhibitors for at least 5 h before being used for experiments.

Western blotting

Cells (about 5×10^4 in total) in a 60 mm dish were washed with ice-cold phosphate-buffered saline (PBS) and lysed in RIPA buffer with protease and phosphatase inhibitors (89900 and A32959, Thermo Fisher Scientific). Concentrated protein samples were separated by electrophoresis on 10% TGX FastCast acrylamide gel (1610172, Bio-Rad) and transferred to PVDF membranes (IPVH00005, Millipore). Membranes were blocked with 5% nonfat milk or 5% BSA in TBST for 1 h and then incubated with primary antibody at 4°C overnight. Primary antibodies included anti-PIK3CB (1:1000; sc-376641, Santa Cruz Biotechnology), anti-PIK3CA antibody (1:500; 4249, Cell Signaling), anti-PIK3CG (1:500; sc166365, Santa Cruz Biotechnology), anti-PIK3CD (1:1000; 34050, Cell Signaling), anti-Akt (1:500; 4691, Cell Signaling), anti-Src (1:2000; 2109, Cell Signaling), anti-Hck (1: 500; 175886, Abcam), anti-Abl1 (1:500; 2862, Cell Signaling), anti-Abl2 (1:1000; ab126256, Abcam), anti-GAPDH (1:1000; AM4300, Thermo Fisher Scientific), anti-tubulin alpha (1:10000; BS1699, Bioworld), pY416-Src antibody (1:1000; 2101, Cell Signaling) and pS473-Akt antibody (1:500; 9271 or 4060, Cell Signaling). Phosphospecific c-Abl (Tyr488) antibody against the peptide KVpYELMRA was a gift from Ingvar Ferby (Uppsala University, Sweden) (Hopkins et al., 2012). After primary antibody incubation, membranes were washed with TBST and subsequently incubated with HRP-linked anti-mouse (1:1000; sc-516102, Santa Cruz Biotechnology) or HRP-linked anti-rabbit (1:2000; 7074S, Cell Signaling) secondary antibody at room temperature for 2 h. After washing with TBST, membranes were developed using ECL western blotting substrate (SG251207, Thermo Fisher Scientific) and exposed to films in the dark room or scanned on myECL Imager (Thermo Fisher Scientific). The full blot images are shown in Fig. S7.

Immunofluorescence staining

Cells were cultured in a glass bottom dish (MatTek) functionalized with collagen-I (50 µg/ml, 30 min coating at 37°C; A1048301, Thermo Fisher Scientific). Freshly prepared paraformaldehyde (PFA, 4% in PBS, 20 min, 37°C) was used to fix the sample. Shortly after fixation, cells were permeabilized with Triton X-100 (0.1% in PBS, 10 min, 37°C), passivated with the blocking buffer (10% donkey serum and 1% BSA) at 4°C overnight and then incubated for the indicated time with the primary antibody at 4°C.

Primary antibodies included anti-paxillin (1:1000, 1 day; 612405, BD Biosciences Pharmingen), anti-vinculin (1:100, 2 days; V9264, Sigma), phosphospecific c-Abl (Tyr488) antibody (1:100, 2 days), and pY416-Src antibody (1:500, 2 days; 2101, Cell Signaling). After being rinsed with 25 ml of PBS, cells were subsequently incubated with secondary antibodies at room temperature for 2 h. Secondary antibodies included Alexa Fluor 488 conjugated anti-mouse, Alexa Fluor 594 conjugated anti-rabbit and DyLight 405 conjugated anti-mouse antibodies (1:1000; A-21202, A-21207 and 35501BID, Thermo Fisher Scientific). CF594-phalloidin or CF680R-phalloidin (1:1000, 4°C overnight; 00045 or 00048, Biotium) was used to stain F-actin.

Microscopy

A total internal reflection fluorescence (TIRF) microscope (Nikon Ti2-E with iLas2) and a spinning-disc confocal microscope (Nikon Ti-E with Yokogawa CSU-X1) were employed to visualize macrophage podosomes. An EMCCD camera (Photometrics Evolve 512), 100× oil immersion lens (1.49 NA), and AOTF-controlled solid-state lasers (50-100 mW) were mounted on the TIRF microscope. MetaMorph software (Molecular Devices) was used to control image acquisitions. Volocity software (Perkin-Elmer) was used to control the spinning-disc confocal microscope, which was equipped with an EMCCD camera (Hamamatsu C9100-23B), 100× oil immersion lens (1.45 NA), and AOTF-controlled solid-state lasers (40–50 mW). Typically, acquisition settings of 10-40% of each laser output, 100 ms exposure time and 80-100% of camera EM gain were utilized. The environmental chamber (37°C and 5% CO_2) was attached to the microscope body for time-lapse imaging. Within each set of samples, identical microscope configurations (laser output, exposure time and camera EM gain) were applied to perform the image acquisition.

Quantification of podosome-forming cells

Podosomes were determined by the identification of distinct core/ring organizations by fluorescence microscopy. Podosome core and ring were labeled with F-actin markers (phalloidin, lifeact and UtrCH) and adhesion markers (paxillin and vinculin), respectively. Typically, the intensity of dot-like F-actin staining at the podosome core was two to five times higher than that of the cytosol background. A macrophage with two or more podosomes was defined as a podosome-forming cell.

Intensity analysis and kymograph

Imaris and ImageJ software were employed for intensity analysis. The F-actin channel was used to define the region of interest (ROI) of the podosome, and mean intensities of other channels within the ROI were measured accordingly. Kymographs and pseudocolor time projections were generated in ImageJ. For the purpose of presentation, each image was uniformly and unbiasedly processed to enhance the contrast.

Degradation assay

Substrata of Cy3-gelatin coated glass were prepared in accordance with manufacturer's instructions (ECM671, Millipore). A glass-bottom dish (MatTek) was functionalized with 1× poly-L-lysine (PLL) at room temperature for 20 min. Cy3-gelatin (4×) was heated at 60°C for 5 min and diluted to 1× with Dulbecco's PBS. Unlabeled gelatin (4×) was also diluted to 1× with Dulbecco's PBS and then mixed with 1× Cy3-gelatin at a volume ratio of 4:1. The mixed Cy3-gelatin was coated onto the PLL-functionalized glass-bottom dish and left for 10 min. Excess Cy3-gelatin mixture was aspirated. The dish was rinsed with PBS and then quenched with complete cell culture medium at room temperature for 30 min. RAW264.7 macrophages were plated on the Cy3-gelatin substrate for 24 h and fixed with 4% PFA for 15 min. After fixation, phalloidin was used to stain the F-actin. Cy3-gelatin degradations were visualized by a spinning-disc confocal microscope. The degraded areas, defined by the regions without Cy3-gelatin, were measured by ImageJ software.

Migration assay

Cell migration assays were performed using transwell cell culture chambers in accordance with the manufacturer's instructions (662638, 8 µm pore diameter; Greiner Bio-One). DMEM with 10% FBS was supplied in the lower compartment of the chamber and served as the chemoattractant. RAW264.7 macrophages were cultured on 50 mm dishes with complete cell culture medium for 72 h and then resuspended in serum-free medium. Resuspended macrophages were loaded in the upper compartment of the chamber. After 24 h, cells were fixed with 4% PFA in PBS for 10 min and stained with crystal violet solution for 5 min. Cells remaining on the inner surface of the chambers were removed with cotton swabs, whereas cells that migrated to the other side of the chambers were imaged using an inverted microscope (Olympus lX71 with a 20× objective and a color CCD DP71 camera). Relative migration capability was defined as the ratio of the number of migrated cells versus the number in the si-Scramble control.

Statistics and reproducibility

One-way ANOVA with Dunnett's test and unpaired two-tailed Student's *t*-test were performed using GraphPad Prism software. Statistical graphs with the mean and standard error of the mean (s.e.m.) were also plotted using GraphPad Prism software. Detailed statistical information, such as calculated F and P values can be found in Table S1. ns, $P>0.1234$, $*P<0.0332$, $**P<0.0021$, $***P<0.0002$ and $****P<0.0001$. Each dataset contains at least three independent biological repeats.

Acknowledgement

The authors would like to thank Dr Ingvar Ferby for pY488-Abl antibody and the technical support from Image Core Facility in Faculty of Medicine at University of Hong Kong.

Competing interests

The authors declare no competing or financial interests.

Author contributions

Conceptualization: C.-h.Y.; Methodology: Y.Z., Z.F., C.-h.Y.; Software: F.C., C.-h.Y.; Validation: Y.Z., Z.F., C.-h.Y.; Formal analysis: Y.Z., Z.F., F.C., C.-h.Y.; Investigation: Y.Z., Z.F., C.-h.Y.; Resources: Y.Z., Z.F., X.L., X.X., C.-h.Y.; Data curation: Y.Z., Z.F., F.C., C.-h.Y.; Writing - original draft: C.-h.Y.; Writing - review & editing: Y.Z., Z.F., C.-h.Y.; Visualization: C.-h.Y.; Supervision: C.-h.Y.; Project administration: C.-h.Y.; Funding acquisition: C.-h.Y.

Funding

This work was supported by Research Grant Council of Hong Kong under award 27110615 and 17124117 (C.-h.Y.).

Supplementary information

Supplementary information available online at
http://jcs.biologists.org/lookup/doi/10.1242/jcs.234385.supplemental

References

Abella, J. V. G., Galloni, C., Pernier, J., Barry, D. J., Kjaer, S., Carlier, M.-F. and Way, M. (2016). Isoform diversity in the Arp2/3 complex determines actin filament dynamics. *Nat. Cell Biol.* **18**, 76-86. doi:10.1038/ncb3286

Albiges-Rizo, C., Destaing, O., Fourcade, B., Planus, E. and Block, M. R. (2009). Actin machinery and mechanosensitivity in invadopodia, podosomes and focal adhesions. *J. Cell Sci.* **122**, 3037-3049. doi:10.1242/jcs.052704

Balla, T. (2013). Phosphoinositides: tiny lipids with giant impact on cell regulation. *Physiol. Rev.* **93**, 1019-1137. doi:10.1152/physrev.00028.2012

Bilanges, B., Posor, Y. and Vanhaesebroeck, B. (2019). PI3K isoforms in cell signalling and vesicle trafficking. *Nat. Rev. Mol. Cell Biol.* **20**, 515-534. doi:10.1038/s41580-019-0129-z

Bourguignon, L. Y. W., Zhu, H., Shao, L. and Chen, Y.-W. (2001). CD44 interaction with c-Src kinase promotes cortactin-mediated cytoskeleton function and hyaluronic acid-dependent ovarian tumor cell migration. *J. Biol. Chem.* **276**, 7327-7336. doi:10.1074/jbc.M006498200

Burkel, B. M., von Dassow, G. and Bement, W. M. (2007). Versatile fluorescent probes for actin filaments based on the actin-binding domain of utrophin. *Cell Motil. Cytoskeleton* **64**, 822-832. doi:10.1002/cm.20226

Calle, Y., Burns, S., Thrasher, A. J. and Jones, G. E. (2006). The leukocyte podosome. *Eur. J. Cell Biol.* **85**, 151-157. doi:10.1016/j.ejcb.2005.09.003

Campellone, K. G. and Welch, M. D. (2010). A nucleator arms race: cellular control of actin assembly. *Nat. Rev. Mol. Cell Biol.* **11**, 237-251. doi:10.1038/nrm2867

Cao, F., Zhou, Y., Liu, X. and Yu, C.-H. (2020). Podosome formation promotes plasma membrane invagination and integrin-beta3 endocytosis on a viscous RGD-membrane. *Commun. Biol.* **3**, 117. doi:10.1038/s42003-020-0843-2

Carmona, G., Perera, U., Gillett, C., Naba, A., Law, A.-L., Sharma, V. P., Wang, J., Wyckoff, J., Balsamo, M., Mosis, F. et al. (2016). Lamellipodin promotes invasive 3D cancer cell migration via regulated interactions with Ena/VASP and SCAR/WAVE. *Oncogene* **35**, 5155-5169. doi:10.1038/onc.2016.47

Chabadel, A., Bañon-Rodríguez, I., Cluet, D., Rudkin, B. B., Wehrle-Haller, B., Genot, E., Jurdic, P., Anton, I. M. and Saltel, F. (2007). CD44 and β3 integrin organize two functionally distinct actin-based domains in osteoclasts. *Mol. Biol. Cell* **18**, 4899-4910. doi:10.1091/mbc.e07-04-0378

Cougoule, C., Le Cabec, V., Poincloux, R., Al Saati, T., Mège, J.-L., Tabouret, G., Lowell, C. A., Laviolette-Malirat, N. and Maridonneau-Parini, I. (2010). Three-dimensional migration of macrophages requires Hck for podosome organization and extracellular matrix proteolysis. *Blood* **115**, 1444-1452. doi:10.1182/blood-2009-04-218735

Dubielecka, P. M., Machida, K., Xiong, X., Hossain, S., Ogiue-Ikeda, M., Carrera, A. C., Mayer, B. J. and Kotula, L. (2010). Abi1/Hssh3bp1 pY213 links Abl kinase signaling to p85 regulatory subunit of PI-3 kinase in regulation of macropinocytosis in LNCaP cells. *FEBS Lett.* **584**, 3279-3286. doi:10.1016/j.febslet.2010.06.029

Duong, L. T. and Rodan, G. A. (2000). PYK2 is an adhesion kinase in macrophages, localized in podosomes and activated by beta(2)-integrin ligation. *Cell Motil. Cytoskeleton* **47**, 174-188. doi:10.1002/1097-0169(200011)47:3<174::AID-CM2>3.0.CO;2-N

El Azzouzi, K., Wiesner, C. and Linder, S. (2016). Metalloproteinase MT1-MMP islets act as memory devices for podosome reemergence. *J. Cell Biol.* **213**, 109-125. doi:10.1083/jcb.201510043

Falkenburger, B. H., Jensen, J. B. and Hille, B. (2010). Kinetics of PIP2 metabolism and KCNQ2/3 channel regulation studied with a voltage-sensitive phosphatase in living cells. *J. Gen. Physiol.* **135**, 99-114. doi:10.1085/jgp.200910345

Fruman, D. A., Chiu, H., Hopkins, B. D., Bagrodia, S., Cantley, L. C. and Abraham, R. T. (2017). The PI3K pathway in human disease. *Cell* **170**, 605-635. doi:10.1016/j.cell.2017.07.029

Gil-Henn, H., Patsialou, A., Wang, Y., Warren, M. S., Condeelis, J. S. and Koleske, A. J. (2013). Arg/Abl2 promotes invasion and attenuates proliferation of breast cancer in vivo. *Oncogene* **32**, 2622-2630. doi:10.1038/onc.2012.284

Hammond, G. R. V., Machner, M. P. and Balla, T. (2014). A novel probe for phosphatidylinositol 4-phosphate reveals multiple pools beyond the Golgi. *J. Cell Biol.* **205**, 113-126. doi:10.1083/jcb.201312072

Hantschel, O. and Superti-Furga, G. (2004). Regulation of the c-Abl and Bcr-Abl tyrosine kinases. *Nat. Rev. Mol. Cell Biol.* **5**, 33-44. doi:10.1038/nrm1280

Hopkins, S., Linderoth, E., Hantschel, O., Suarez-Henriques, P., Pilia, G., Kendrick, H., Smalley, M. J., Superti-Furga, G. and Ferby, I. (2012). Mig6 is a sensor of EGF receptor inactivation that directly activates c-Abl to induce apoptosis during epithelial homeostasis. *Dev. Cell* **23**, 547-559. doi:10.1016/j.devcel.2012.08.001

Hoshino, D., Branch, K. M. and Weaver, A. M. (2013). Signaling inputs to invadopodia and podosomes. *J. Cell Sci.* **126**, 2979-2989. doi:10.1242/jcs.079475

Innocenti, M., Zucconi, A., Disanza, A., Frittoli, E., Areces, L. B., Steffen, A., Stradal, T. E., Di Fiore, P. P., Carlier, M. F. and Scita, G. (2004). Abi1 is essential for the formation and activation of a WAVE2 signalling complex. *Nat. Cell Biol.* **6**, 319-327. doi:10.1038/ncb1105

Insall, R. H. and Weiner, O. D. (2001). PIP3, PIP2, and cell movement–similar messages, different meanings? *Dev. Cell* **1**, 743-747. doi:10.1016/S1534-5807(01)00086-7

Ismail, A. M., Padrick, S. B., Chen, B., Umetani, J. and Rosen, M. K. (2009). The WAVE regulatory complex is inhibited. *Nat. Struct. Mol. Biol.* **16**, 561-563. doi:10.1038/nsmb.1587

Jain, S. K., Susa, M., Keeler, M. L., Carlesso, N., Druker, B. and Varticovski, L. (1996). PI 3-kinase activation in BCR/abl-transformed hematopoietic cells does not require interaction of p85 SH2 domains with p210 BCR/abl. *Blood* **88**, 1542-1550. doi:10.1182/blood.V88.5.1542.1542

Kanai, F., Liu, H., Field, S. J., Akbary, H., Matsuo, T., Brown, G. E., Cantley, L. C. and Yaffe, M. B. (2001). The PX domains of p47phox and p40phox bind to lipid products of PI(3)K. *Nat. Cell Biol.* **3**, 675-678. doi:10.1038/35083070

Khatri, A., Wang, J. and Pendergast, A. M. (2016). Multifunctional Abl kinases in health and disease. *J. Cell Sci.* **129**, 9-16. doi:10.1242/jcs.175521

Lam, A. J., St-Pierre, F., Gong, Y., Marshall, J. D., Cranfill, P. J., Baird, M. A., McKeown, M. R., Wiedenmann, J., Davidson, M. W., Schnitzer, M. J. et al. (2012). Improving FRET dynamic range with bright green and red fluorescent proteins. *Nat. Methods* **9**, 1005-1012. doi:10.1038/nmeth.2171

Legate, K. R., Wickstrom, S. A. and Fassler, R. (2009). Genetic and cell biological analysis of integrin outside-in signaling. *Genes Dev.* **23**, 397-418. doi:10.1101/gad.1758709

Linder, S. and Kopp, P. (2005). Podosomes at a glance. *J. Cell Sci.* **118**, 2079-2082. doi:10.1242/jcs.02390

Linder, S., Nelson, D., Weiss, M. and Aepfelbacher, M. (1999). Wiskott-Aldrich syndrome protein regulates podosomes in primary human macrophages. *Proc. Natl. Acad. Sci. USA* **96**, 9648-9653. doi:10.1073/pnas.96.17.9648

Linder, S., Hufner, K., Wintergerst, U. and Aepfelbacher, M. (2000). Microtubule-dependent formation of podosomal adhesion structures in primary human macrophages. *J. Cell Sci.* **113**, 4165-4176.

Manning, B. D. and Toker, A. (2017). AKT/PKB signaling: navigating the network. *Cell* **169**, 381-405. doi:10.1016/j.cell.2017.04.001

Mitra, S. K. and Schlaepfer, D. D. (2006). Integrin-regulated FAK-Src signaling in normal and cancer cells. *Curr. Opin. Cell Biol.* **18**, 516-523. doi:10.1016/j.ceb.2006.08.011

Murphy, D. A. and Courtneidge, S. A. (2011). The 'ins' and 'outs' of podosomes and invadopodia: characteristics, formation and function. *Nat. Rev. Mol. Cell Biol.* **12**, 413-426. doi:10.1038/nrm3141

Oikawa, T., Itoh, T. and Takenawa, T. (2008). Sequential signals toward podosome formation in NIH-src cells. *J. Cell Biol.* **182**, 157-169. doi:10.1083/jcb.200801042

Papayannopoulos, V., Co, C., Prehoda, K. E., Snapper, S., Taunton, J. and Lim, W. A. (2005). A polybasic motif allows N-WASP to act as a sensor of PIP2 density. *Mol. Cell* **17**, 181-191. doi:10.1016/j.molcel.2004.11.054

Parsons, J. T., Horwitz, A. R. and Schwartz, M. A. (2010). Cell adhesion: integrating cytoskeletal dynamics and cellular tension. *Nat. Rev. Mol. Cell Biol.* **11**, 633-643. doi:10.1038/nrm2957

Pollard, T. D. (2007). Regulation of actin filament assembly by Arp2/3 complex and formins. *Annu. Rev. Biophys. Biomol. Struct.* **36**, 451-477. doi:10.1146/annurev.biophys.35.040405.101936

Ren, R., Ye, Z. S. and Baltimore, D. (1994). Abl protein-tyrosine kinase selects the Crk adapter as a substrate using SH3-binding sites. *Genes Dev.* **8**, 783-795. doi:10.1101/gad.8.7.783

Rohatgi, R., Ho, H.-H. and Kirschner, M. W. (2000). Mechanism of N-WASP activation by CDC42 and phosphatidylinositol 4, 5-bisphosphate. *J. Cell Biol.* **150**, 1299-1310. doi:10.1083/jcb.150.6.1299

Schachtner, H., Calaminus, S. D. J., Thomas, S. G. and Machesky, L. M. (2013). Podosomes in adhesion, migration, mechanosensing and matrix remodeling. *Cytoskeleton* **70**, 572-589. doi:10.1002/cm.21119

Sharma, V. P., Eddy, R., Entenberg, D., Kai, M., Gertler, F. B. and Condeelis, J. (2013). Tks5 and SHIP2 regulate invadopodium maturation, but not initiation, in breast carcinoma cells. *Curr. Biol.* **23**, 2079-2089. doi:10.1016/j.cub.2013.08.044

Songyang, Z., Shoelson, S. E., Chaudhuri, M., Gish, G., Pawson, T., Haser, W. G., King, F., Roberts, T., Ratnofsky, S., Lechleider, R. J. et al. (1993). SH2 domains recognize specific phosphopeptide sequences. *Cell* **72**, 767-778. doi:10.1016/0092-8674(93)90404-E

Taylor, M. J., Perrais, D. and Merrifield, C. J. (2011). A high precision survey of the molecular dynamics of mammalian clathrin-mediated endocytosis. *PLoS Biol.* **9**, e1000604. doi:10.1371/journal.pbio.1000604

Várnai, P. and Balla, T. (1998). Visualization of phosphoinositides that bind pleckstrin homology domains: calcium- and agonist-induced dynamic changes and relationship to myo-[3H]inositol-labeled phosphoinositide pools. *J. Cell Biol.* **143**, 501-510. doi:10.1083/jcb.143.2.501

Vazquez, F., Ramaswamy, S., Nakamura, N. and Sellers, W. R. (2000). Phosphorylation of the PTEN tail regulates protein stability and function. *Mol. Cell. Biol.* **20**, 5010-5018. doi:10.1128/MCB.20.14.5010-5018.2000

Villefranc, J. A., Amigo, J. and Lawson, N. D. (2007). Gateway compatible vectors for analysis of gene function in the zebrafish. *Dev. Dyn.* **236**, 3077-3087. doi:10.1002/dvdy.21354

Yu, C.-H., Rafiq, N. B. M., Krishnasamy, A., Hartman, K. L., Jones, G. E., Bershadsky, A. D. and Sheetz, M. P. (2013). Integrin-matrix clusters form podosome-like adhesions in the absence of traction forces. *Cell Reports* **5**, 1456-1468. doi:10.1016/j.celrep.2013.10.040

Yuan, Z.-M., Utsugisawa, T., Huang, Y., Ishiko, T., Nakada, S., Kharbanda, S., Weichselbaum, R. and Kufe, D. (1997). Inhibition of phosphatidylinositol 3-kinase by c-Abl in the genotoxic stress response. *J. Biol. Chem.* **272**, 23485-23488. doi:10.1074/jbc.272.38.23485

Zhang, Y., Cao, F., Zhou, Y., Feng, Z., Sit, B., Krendel, M. and Yu, C.-H. (2019). Tail domains of myosin-1e regulate phosphatidylinositol signaling and F-actin polymerization at the ventral layer of podosomes. *Mol. Biol. Cell* **30**, 622-635. doi:10.1091/mbc.E18-06-0398

Zhao, P., Xu, Y., Wei, Y., Qiu, Q., Chew, T.-L., Kang, Y. and Cheng, C. (2016). The CD44s splice isoform is a central mediator for invadopodia activity. *J. Cell Sci.* **129**, 1355-1365. doi:10.1242/jcs.171959